CARBON letters

Original Articles
Carbon Letters Vol. 27, 12-17 (2018)

The effect of pore structure and surface properties of carbon nanotube films on the performance of a lithium sulfur battery

Hyeonjun Song[1], Yunjae Hwang[1], Vimal Tiwari Kumar[2] and Youngjin Jeong[1,2,♠]

[1]Department of Information Communication, Materials, and Chemistry Convergence Technology, Soongsil University, Seoul 06978, Korea
[2]Department of Organic Materials and Fiber Engineering, Soongsil University, Seoul 06978, Korea

Article Info
Received 23 October 2017
Accepted 21 December 2017

♠Corresponding Author
E-mail: yjeong@ssu.ac.kr

Open Access
DOI: http://dx.doi.org/10.5714/CL.2018.27.012

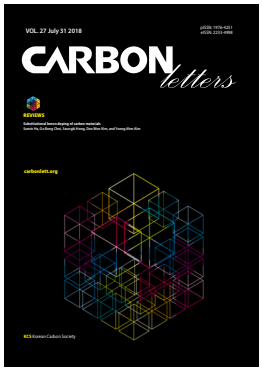

http://carbonlett.org

pISSN: 1976-4251
eISSN: 2233-4998

Abstract

We fabricated a Li-S battery with post-treated carbon nanotube (CNT) films which offered better support for sulfur, and investigated the effect of the surface properties and pore structure of the post-treated CNT films on Li-S battery performance. Post-treatments, i.e., acid treatment, unzip process and cetyltrimethylammonium bromide (CTAB) treatment, effectively modified the surface properties and pore structure of the CNT film. The modified pore structure impacted the ability of the CNT films to accommodate the catholyte, resulting in an increase in initial discharge capacity.

Key words: Carbon nanotube, Lithium sulfur battery, pore structure, surface proeperty

1. Introduction

One of the most promising candidates for the next generation battery is the lightweight and high capacity lithium sulfur (Li-S) battery with highly conducting carbon nanotube (CNT) films as the electrode material. Electric vehicles (EVs) and portable information technology (IT) devices demand significant improvements in the rechargeable battery, particularly higher energy density. Conventional lithium-ion batteries (LIBs) which are usually based on the $LiCoO_2$/graphite and $LiFePO_4$/graphite system are not suitable as a power source for such applications, because of their low energy density [1-5]. Numerous investigations are underway to develop a rechargeable battery with suitable high energy density to replace the conventional LIBs. Li-S batteries have recently received significant interest because they have demonstrated a high energy density of 2600 Wh kg^{-1} and a high theoretical capacity of 1675 mAh g^{-1} [6-8]. Moreover, the low price, nontoxicity and light weight of the sulfur as a cathode material for Li-S batteries makes it a more attractive for practical applications [9-11].

Despite its promise, Li-S batteries still have some problems that hinder its commercialization. Low capacity retention due to the polysulfide shuttling phenomenon offsets several advantages of the Li-S battery. Polysulfides (Li_2S_x, $1 \leq x \leq 8$), which are intermediate products during the redox reaction between lithium and sulfur, easily dissolve into the electrolyte, and shuttle between sulfur and lithium in what is known as the shuttling phenomenon [12]. The polysulfide shuttling phenomenon results in poor cyclability of the Li-S batteries, because low-order polysulfides such as Li_2S and Li_2S_2 which are formed by the reaction between the dissolved polysulfides and lithium, become an insulating layer on the surface of the Li metal [13-15].

To overcome this problem, studies have investigated ways of preventing the polysulfide shuttling phenomenon. The typical method involves disturbing the migration of the polar polysulfides using carbon materials with appropriate functional groups [16,17]. A free-standing sulfur/dehydrogenated polyacrylonitrile/multiwalled CNT composite [18], sulfur embedded tube-in-tube carbon structure [19] and CNT-PEI/sulfur composite [20] for high performance lithium sulfur batteries were prepared by using a suitable conductive matrix

to bind sulfur. This enables the uniform distribution of sulfur and high conductivity of the CNT network with excellent mechanical stability. Sulfur composites with mesoporous CNT [21] and partially unzipped CNT (U-CNT) [22] as cathodes for Li-S batteries were synthesized by incorporating sulfur into a treated CNT network with high sulfur loading, and demonstrated excellent electrochemical performance. Zheng et al. [17], in preparing a sulfur electrode, introduced an AAO template by coating carbon on the template and then loading sulfur, modifying the carbon and etching the AAO template. This modified hollow carbon electrode showed 80% capacity retention for 300 cycles [17]. However, the complicated process limits the practical applications of such a system.

In this study, we explored the effects of pore structure and surface properties of CNT film, which acted as a sulfur support, on Li-S battery performance. Various post-treatments were performed on the CNT film in order to modify the pore structure and surface properties of the CNT film. Analysis of the post-treated CNT films and the electrochemical performance of the Li-S device prepared with the post-treated CNT films was conducted in this study.

2. Experimental

2.1. Post-treatment of the CNT film

The CNT film was synthesized continuously via direct spinning method as previously reported [23]. The precursor solution, which contains acetone (99.7%, Samchun Chemical, Korea), ferrocene (98%, Sigma Aldrich, USA), thiophene (≥99%, Sigma Aldrich), and polysorbate_20 (Sigma Aldrich) was injected into a 1200°C reactor at a rate of 10 mL h^{-1} with a carrier gas (H_2, 1000 sccm) [23]. To obtain acid treated CNT (A-CNT) film, the CNT film was suspended in a 3 to 1 mixture of sulfuric acid and nitric acid (60%, Samchun Chemical) at 50°C for 30 min. To obtain the U-CNT film, the CNT film was soaked in sulfuric acid (96%, Samchun Chemical) for 5 h and then treated with 500 wt% potassium permanganate ($KMnO_4$, 97%, Sigma Aldrich) for 1 h [24]. When the color of the CNT film changed to brownish during heating at 55°C for 30 min, the treated CNT film was rinsed with deionized (DI) water. The A-CNT film and the U-CNT films were then freeze-dried and heated at 400°C under atmospheric conditions to remove residual moisture. To introduce cationic ions onto the surface of the CNT films, cetyltrimethylammonium bromide (CTAB 99+ %, Samchun Chemical) was added to DI water (100 mL) to make a dilute CTAB solution. The CNT film was dipped in the dilute CTAB solution for 3 h. After that, the CTAB treated CNT (C-CNT) film was freeze-dried and heated at 120°C for 12 h.

2.2. Fabrication of a catholyte@CNT film electrode

Lithium trifluoromethanesulfonate ($LiCF_3SO_3$, 98%, TCI) of 1 M was dissolved in a 1:1 (v/v) mixture of 1,3-dioxolane (DOL; 99.5%, Acros) and ethylene glycol dimethyl ether (DME; 99.5%, Acros) with a 0.1 M lithium nitrate ($LiNO_3$, 99%, Acros) additive to prepare an electrolyte. Catholyte (Li_2S_6) was synthesized by reacting sulfur with Li_2S (5:1 in molarity ratio) in the electrolyte at 55°C for 24 h. The catholyte@CNT film electrode was prepared by dropping a 40 μL of catholyte onto the modified CNT film. All these processes were conducted in an Ar-filled glove box (Korea Kiyon, Korea).

2.3. Electrochemical measurement

The electrochemical performance of the catholyte@CNT film was evaluated by assembling a coin cell (CR 2032, MTI Korea). The catholyte@CNT film electrode and Li metal were used as a working electrode and a counter electrode, respectively. A microporous trilayer membrane (PP/PE/PP, Celgard 2325) was used as the separator. All cells were assembled in an Ar-filled glove box. Galvanostatic charge/discharge tests were carried out at various current densities over the voltage range 1.7 to 2.6 V (vs. Li/LI^+) using a charge/discharge cycler (Shin Corp., TOSAT-3100U).

2.4. Characterization

The morphologies of the post-treated CNT films were analyzed in a field emission scanning electron microscopy (JSM-6700F, JEOL). Transmission electron microscopy images were taken using a FEI Tecnai G2 F20 electron microscope operating at 200 kV. The surface properties of the post-treated CNT films were evaluated by Fourier-transform infrared spectroscopy (FT-IR; VERTEX, Bruker) using the ATR method in the range of 600 to 4000 cm^{-1} and contact angle (DST100, KRUSS). X-ray photoelectron spectroscopy analysis was carried out with a Kratos, AXIS Nova with Al-Kα radiation. The surface area and pore size distribution of the post-treated CNT films were measured with Micromeritics ASAP 2020, and the pore size was calculated by the Barrett-Joyner-Halenda method. The 0.1 M catholyte was used for the UV-Vis measurement. UV-visible adsorption spectroscopic data was collected in the range of 200 to 800 nm via UV-Vis spectrophotometer (UV-3600, SHIMADZU).

3. Results and Discussion

3.1. Morphological studies of the post-treated CNT film

The morphology images of the post-treated CNT film, which not only acted as a sulfur support but also worked as a current collector, are presented in Fig. 1. Fig. 1a shows that the pristine CNT film consists of long CNT bundles which form a porous network structure. This porous structure of the CNT film facilitates the infiltration of catholyte containing sulfur inside the CNT film, enabling easy electron conduction by sulfur without a polymeric binder and a conductive agent. The A-CNT film was observed to have a denser morphology than those of the pristine CNT film as shown in Fig. 1b. The acid mixture solvent causes densification of the CNT film due to bundling of the CNTs. This bundling effect in CNT film has been reported in the previous literature [25] and is attributed to capillary forces.

As seen in Fig. 1c, the U-CNT film also exhibits a dense morphology, because the CNT bundles open to become a graphene

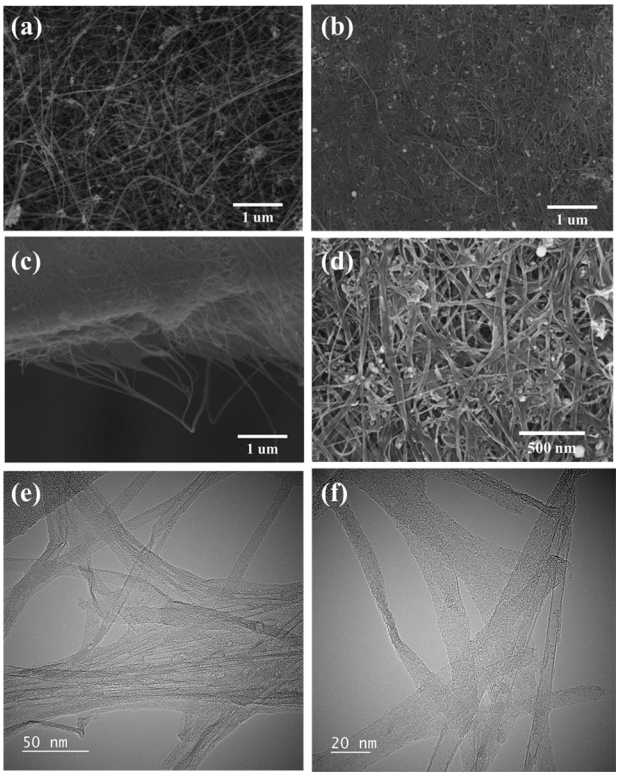

Fig. 1. Scanning electron microscopy images of the post-treated CNT film. (a) The pristine CNT film, (b) A-CNT film, (c) U-CNT film (inset: high magnification) and (d) C-CNT film. (e, f) Transmission electron microscopy images of U-CNT film.

nanoribbon (GNR; inset image in Fig. 1e and f), and densification occurs due to the bundling effect after the unzip process. In contrast, in the C-CNT film, no morphology difference was observed compared to the pristine CNT film, because the CTAB treatment process does not damage the structure of the CNT film, as shown in Fig. 1d. The morphology of the C-CNT film shows CNT bundles covered with CTAB forming a network structure like the pristine CNT film.

3.2. Analysis of the post-treated CNT films

To confirm the effect of the post-treatment on the pore structure of the CNT film, the surface area and the pore size distribution were measured using a BET analysis. The surface area of the pristine CNT film and the post treated CNT films are listed in Table 1. The surface area of the A-CNT film was 212 m^2 g^{-1}, which is slightly higher than those of the pristine CNT film (195 m^2 g^{-1}). The increase in the surface area is due to damage to the CNT bundles caused by the acid treatment.

It is interesting that the surface area of the U-CNT film (175 m^2 g^{-1}) was lower than those of the pristine CNT film, even though the unzip treatment is harsher process than the acid treatment. The differences in the surface area changes are probably due to the variable degree of the damage caused to the CNT bundles. The acid treatment caused defects in the CNT bundles, but it did not destroy the structure of the CNT film. Therefore, the defects on the CNT bundle might increase the surface area

Table 1. Surface areas of the pristine CNT film and the post-treated CNT films

Sample	Surface area (m^2 g^{-1})
Pristine CNT film	195
A-CNT film	212
U-CNT film	175
C-CNT film	111

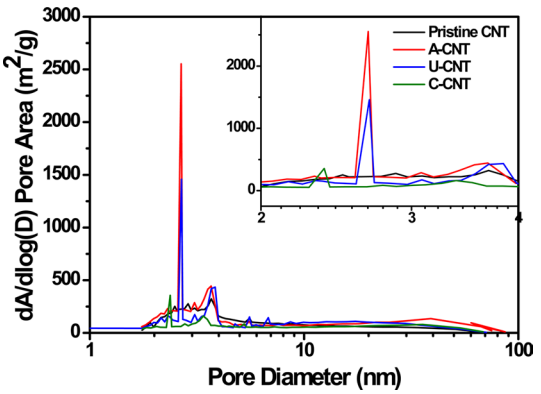

Fig. 2. Pore size distribution of the pristine CNT film and the post-treated CNT films.

of the CNT film, whereas, the cylindrical CNTs were fully converted to the GNRs by the unzip process, as seen in Fig. 1e and f.

The GNR can block the pores in the CNT film, so the unzip process leads to a decrease in the surface area of the CNT film. The C-CNT film showed a much smaller surface area than those of the pristine CNT film. The reason behind the decrease in surface area is evident from the morphology of the C-CNT film in Fig. 1d. The CTAB, which is covering the CNT bundles, blocked the pores in the CNT film, which leads to the decrease in surface area.

Fig. 2 shows the pore distribution of the pristine CNT film and the post treated CNT films. The 2.7 nm pore size (mesopores) conspicuously increased after the acid treatment and unzip process. In contrast, no variation in pore distribution was observed after the CTAB treatment. These results suggest that the damage to the CNT bundles not only affected the surface area but also affected the pore distribution.

In order to observe the surface properties of the post-treated CNT films, FT-IR measurements and contact angle measurements were conducted and the corresponding results are presented in Fig. 3a. The FT-IR spectra of the A-CNT film and U-CNT film generally did not show strong features. The appearance of the characteristic peaks of C=O at 1735 cm^{-1} confirmed the presence of carboxylic groups. However, the presence of the C=O stretching band (1700–1760 cm^{-1}) [25], the COO^- stretching band and C=C stretching band (1500–1580 cm^{-1}) [26] indicated that the carboxylic groups were introduced to the surface of the CNT film by the acid treatment and the unzip process.

Additionally, the contact angle decreased in both samples. The band at 1400–1500 cm^{-1} is attributed to the C-H bending

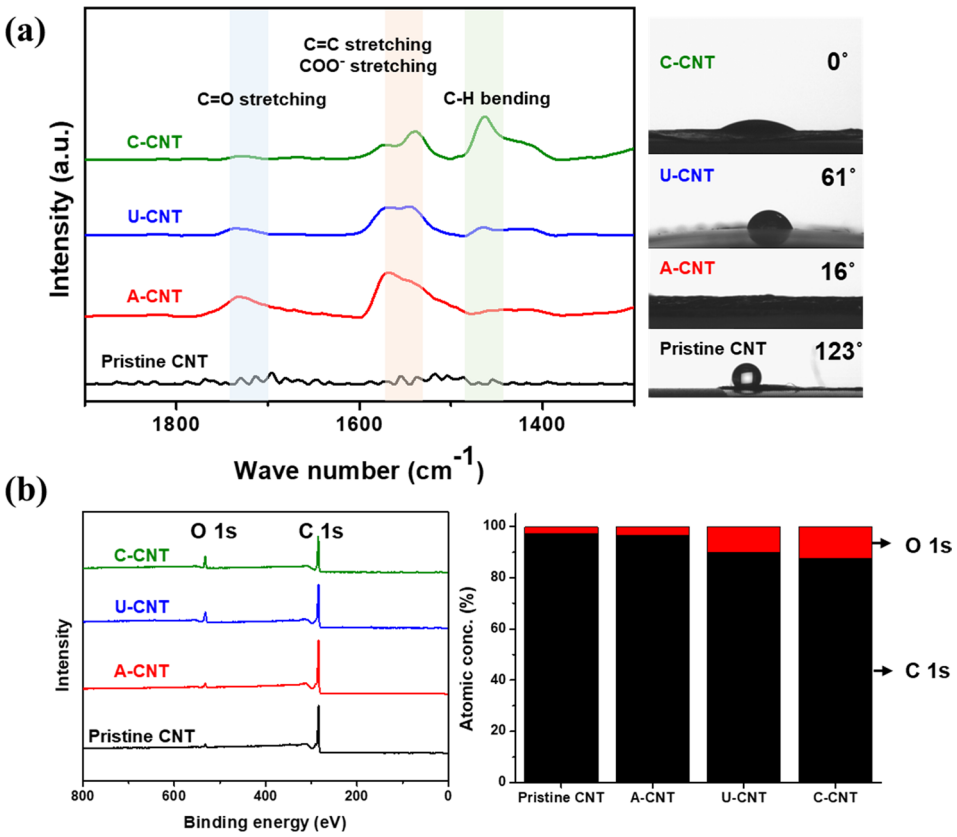

Fig. 3. (a) FT-IR spectra and water contact angle of Pristine CNT film and post-treated CNT films. (b) X-ray photoelectron spectroscopy peaks and atomic concentrations of Pristine CNT film and post-treated CNT films.

of $CH3\text{-}N^+$ [27], which was introduced by the CTAB treatment on the surface of the CNT film. Also, the contact angle of the C-CNT film decreased compared to those of the pristine CNT film. Furthermore, the concentration of oxygen in the CNT film increased after post-treatments as shown in Fig. 3b. These results suggest that the surface properties of the pristine CNT film were effectively modified by the post-treatments.

3.3. Electrochemical properties of Li-S battery with the post-treated CNT films

According to previous studies, the surface polarity of the sulfur electrode suppresses the migration of the polysulfide [16,17]. It was expected that the CNT film with the functional groups on the surface introduced by the post-treatment would suppress the diffusion of the catholyte in the CNT film into the electrolyte. The difference in the concentration of polysulfides between the catholyte and the electrolyte leads to the diffusion of the polysulfide from the catholyte to the electrolyte, according to Fick's law.

The increase in polysulfide dissolution in the electrolyte results in a decrease in specific capacity and capacity retention, thus the concentration of the polysulfide in the electrolyte could serve as a yardstick for the Li-S electrode. To confirm this assumption, we soaked the post-treated CNT films, which absorbed the catholyte, into the electrolyte for 1h, and measured the concentration of the polysulfide in the electrolyte by UV-vis spectroscopy. Based on the contact angle measurements in Fig. 3, the concentrations of polysulfide in the electrolyte were expected to increase in the following order: A-CNT film > C-CNT film > U-CNT film. However, the C-CNT film had the highest polysulfide concentration, as shown in Fig. 4. In addition, the concentration of the A-CNT film and the U-CNT film were almost the same, although the degree of polarity was not the same.

It is thus inferred that the A-CNT film and U-CNT film, with a mainly mesoporous pore structure, have a similar ability to accommodate the catholyte. In contrast, the C-CNT film, where the surface area was reduced without changing the pore structure, exhibited the poorest ability to accommodate the catholyte. These results are contrary to previous studies [16,17] which claimed that the surface polarity of the electrode affected the migration of the polysulfide.

The present results show that the pore structure of the Li-S electrode more significantly affects the migration of the polysulfide than the surface polarity of the Li-S electrode.

Coin cells were fabricated to evaluate the cyclability of prepared Li-S electrodes. Fig. 5 shows the cycle stability test results of the pristine CNT film and the post-treated CNT films. The initial discharge capacities of the A-CNT film, the U-CNT films and the C-CNT film were 1131, 1003 and 980 mAh g^{-1}, respectively. The highest initial discharge capacity of the A-CNT film might be due to the increased surface area and the mesoporous structure of the A-CNT film, which is favorable to the accommodation of the catholyte.

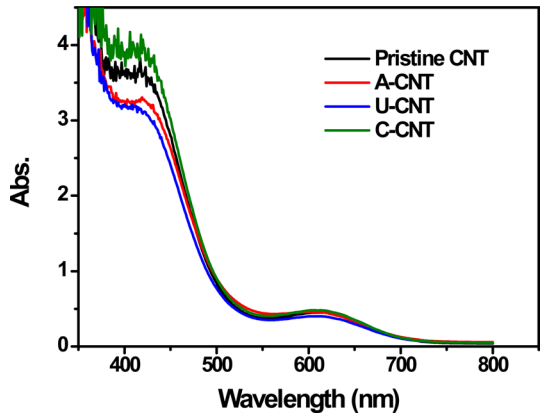

Fig. 4. UV-vis analysis of the pristine CNT film and the post-treated CNT films.

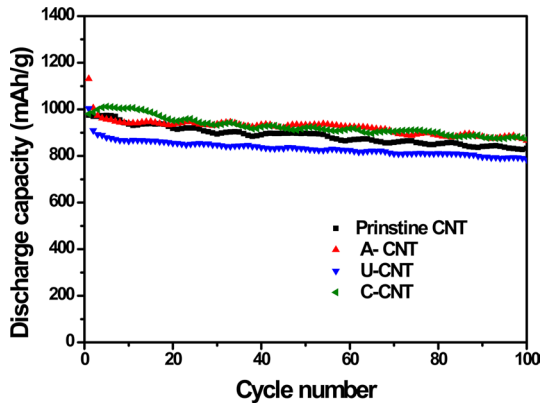

Fig. 5. Cycle performance of the pristine CNT film and the post-treated CNT films at 0.5C.

Also, the lowest initial discharge capacity of the C-CNT film might have been caused by its low surface area. All of the Li-S cells with post-treated CNT films showed a similar level of capacity retention. This finding reveals that the surface polarity of the Li-S electrode does not significantly suppresses the shuttling phenomenon of the polysulfide, as previously reported [16,17].

4. Conclusions

In this study, we fabricated Li-S electrodes with catholyte-modified CNT films and investigated their electrochemical properties. Through various post-treatments, functional groups were introduced on the surface of the CNT film and the pore structure of the CNT film was modified. The A-CNT film and U-CNT film, which had a mesoporous structure, showed good ability to accommodate the catholyte, which contributed to a high initial discharge capacity. However, the surface property of the electrode was not observed to affect the shuttling phenomenon of the polysulfide. Consequentially, the pore structure of the electrode was determined to be more important than the surface property of the electrode for improving the performance of the Li-S battery.

Conflict of Interest

No potential conflict of interest relevant to this article was reported.

Acknowledgements

The authors gratefully acknowledge the financial support provided by Defense Acquisition Program Administration and Agency for Defense Development under the contract 17-CM-MA-21.

References

[1] Gwon H, Hong J, Kim H, Seo DH, Jeon S, Kang K. Recent progress on flexible lithium rechargeable batteries. Energy Environ Sci, **7**, 538 (2014). https://doi.org/10.1039/C3EE42927J.

[2] Tarascon JM, Armand M. Issues and challenges facing rechargeable lithium batteries. Nature, **414**, 359 (2001). https://doi.org/10.1038/35104644.

[3] Lou XW, Deng D, Lee JY, Feng J, Archer LA. Self-supported formation of needlelike Co_3O_4 nanotubes and their application as lithium-ion battery electrodes. Adv Mater, **20**, 258 (2008). https://doi.org/10.1002/adma.200702412.

[4] Yao Y, McDowell MT, Ryu I, Wu H, Liu N, Hu L, Cui Y. Interconnected silicon hollow nanospheres for lithium-ion battery anodes with long cycle life. Nano Lett, **11**, 2949 (2011). https://doi.org/10.1021/nl201470j.

[5] Ng SH, Wang J, Guo ZP, Chen J, Wang GX, Liu HK. Single wall carbon nanotube paper as anode for lithium-ion battery. Electrochim Acta, **51**, 23 (2005). https://doi.org/10.1016/j.electacta.2005.04.045.

[6] Ji X, Nazar LF. Advances in Li–S batteries. J Mater Chem, **20**, 9821 (2010). https://doi.org/10.1039/B925751A.

[7] Peramunage D, Licht S. A solid sulfur cathode for aqueous batteries. Science, **261**, 1029 (1993). https://doi.org/10.1126/science.261.5124.1029.

[8] Wang H, Yang Y, Liang Y, Robinson JT, Li Y, Jackson A, Dai H. Graphene-wrapped sulfur particles as a rechargeable lithium-sulfur battery cathode material with high capacity and cycling stability. Nano Lett, **11**, 2644 (2011). https://doi.org/10.1021/nl200658a.

[9] Guo R, Shi P, Cheng X, Ma Y, Tan Z. Effect of Ag additive on the performance of $LiNi_1/3Co_1/3Mn_1/3O_2$ cathode material for lithium ion battery. J Power Sources, **189**, 2 (2009). https://doi.org/10.1016/j.jpowsour.2009.01.016.

[10] Yang Y, McDowell MT, Jackson A, Cha JJ, Hong SS, Cui Y. New nanostructured Li_2S/silicon rechargeable battery with high specific energy. Nano Lett, **10**, 1486 (2010). https://doi.org/10.1021/nl100504q.

[11] Liang C, Dudney NJ, Howe JY. Hierarchically structured sulfur/carbon nanocomposite material for high-energy lithium battery. Chem Mater, **21**, 4724 (2009). https://doi.org/10.1021/cm902050j.

[12] Jayaprakash N, Shen J, Moganty SS, Corona A, Archer LA. Porous hollow carbon@sulfur composites for high-power lithium–sulfur batteries. Angew Chem, **123**, 26 (2011). https://doi.org/10.1002/ange.201100637.

[13] Mikhaylik YV, Akridge JR. Polysulfide shuttle study in the Li/S battery system. J Electrochem Soc, **151**, A1969 (2004). https://doi.org/10.1149/1.1806394.

[14] Song MS, Han SC, Kim HS, Kim JH, Kim KT, Kang YM, Ahn HJ, Dou SX, Lee JY. Effects of nanosized adsorbing material on electrochemical properties of sulfur cathodes for Li/S secondary batteries. J Electrochem Soc, **151**, A791 (2004). https://doi.org/10.1149/1.1710895.

[15] Evers S, Nazar LF. New approaches for high energy density lithium–sulfur battery cathodes. Acc Chem Res, **46**, 1135 (2012). https://doi.org/10.1021/ar3001348.

[16] Su YS, Fu Y, Manthiram A. Self-weaving sulfur–carbon composite cathodes for high rate lithium–sulfur batteries. Phys Chem Chem Phys, **14**, 14495 (2012). https://doi.org/10.1039/C2CP42796F.

[17] Zheng G, Zhang Q, Cha JJ, Yang Y, Li W, Seh ZW, Cui Y. Amphiphilic surface modification of hollow carbon nanofibers for improved cycle life of lithium sulfur batteries. Nano Lett, **13**, 1265 (2013). https://doi.org/10.1021/nl304795g.

[18] Mentbayeva A, Belgibayeva A, Umirov N, Zhang Y, Taniguchi I, Kurmanbayeva I, Bakenov Z. High performance freestanding composite cathode for lithium-sulfur batteries. Electrochim Acta, **217**, 242 (2016). https://doi.org/10.1016/j.electacta.2016.09.082.

[19] Jin F, Xiao S, Lu L, Wang Y. Efficient activation of high-loading sulfur by small CNTs confined inside a large CNT for high-capacity and high-rate lithium–sulfur batteries. Nano Lett, **16**, 440 (2015). https://doi.org/10.1021/acs.nanolett.5b04105.

[20] Ma LL, Zhuang HL, Wei S, Hendrickson KE, Kim MS, Cohn G, Hennig RG, Archer LA. Enhanced Li–S batteries using amine-functionalized carbon nanotubes in the cathode. ACS Nano, **10**, 1050 (2015). https://doi.org/10.1021/acsnano.5b06373.

[21] Sun L, Wang D, Luo Y, Wang K, Kong W, Wu Y, Zhang L, Jiang K, Li Q, Zhang Y, Wang J, Fan S. Sulfur embedded in a mesoporous carbon nanotube network as a binder-free electrode for high-performance lithium–sulfur batteries. ACS Nano, **10**, 1300 (2015). https://doi.org/10.1021/acsnano.5b06675.

[22] Jeong YC, Lee K, Kim T, Kim JH, Park J, Cho YS, Yang SJ, Park CR. Partially unzipped carbon nanotubes for high-rate and stable lithium–sulfur batteries. J Mater Chem A, **4**, 819 (2016). https://doi.org/10.1039/C5TA07818K.

[23] Song J, Kim S, Yoon S, Cho D, Jeong Y. Enhanced spinnability of carbon nanotube fibers by surfactant addition. Fibers Polym, **15**, 762 (2014). https://doi.org/10.1007/s12221-014-0762-2.

[24] Kosynkin DV, Higginbotham AL, Sinitskii A, Lomeda JR, Dimiev A, Price BK, Tour JM. Longitudinal unzipping of carbon nanotubes to form graphene nanoribbons. Nature, **458**, 872 (2009). https://doi.org/10.1038/nature07872.

[25] Liu Z, Ci L, Kar S, Ajayan PM, Lu JQ. Fabrication and electrical characterization of densified carbon nanotube micropillars for IC interconnection. IEEE Trans Nanotechnol, **8**, 196 (2009). https://doi.org/10.1109/TNANO.2008.2011774.

[26] Avilés F, Cauich-Rodríguez JV, Moo-Tah L, May-Pat A, Vargas-Coronado R. Evaluation of mild acid oxidation treatments for MWCNT functionalization. Carbon, **47**, 2970 (2009). https://doi.org/10.1016/j.carbon.2009.06.044.

[27] Gutiérrez-Becerra A, Barcena-Soto M, Soto V, Arellano-Ceja J, Casillas N, Prévost S, Noirez L, Gradzielski M, Escalante JI. Structure of reverse microemulsion-templated metal hexacyanoferrate nanoparticles. Nanoscale Res Lett, **7**, 83 (2012). https://doi.org/10.1186/1556-276X-7-83.